

Relationship Between Controllability Scoring and Optimal Experimental Design

Kazuhiro Sato

Department of Mathematical Informatics, Graduate School of Information Science and Technology

The University of Tokyo

Tokyo 113-8656, Japan

email: kazuhiro@mist.i.u-tokyo.ac.jp

Abstract—Controllability scores provide control-theoretic centrality measures that quantify the relative importance of state nodes in networked dynamical systems. We establish a structural connection between finite-time controllability scoring and approximate optimal experimental design (OED): the finite-time controllability Gramian decomposes additively across nodes, yielding an affine matrix model of the same form as the information-matrix model in OED. This yields a direct correspondence between the volumetric controllability score (VCS) and D-optimality, and between the average energy controllability score (AECS) and A-optimality, implying that the classical D/A invariance gap has a direct analogue in controllability scoring. By contrast, we point out that controllability scoring typically admits a unique optimizer, unlike approximate-OED formulations. Finally, we uncover a long-horizon phenomenon with no OED counterpart: source-like state nodes without a negative self-loop can be increasingly downweighted by AECS as the horizon grows. Two numerical examples corroborate this long-horizon downweighting behavior.

Index Terms—Controllability score, networked dynamical system, optimal experimental design

I. INTRODUCTION

Assessing the importance of individual state nodes in a dynamical network is a recurring need in control and network science [1]–[4]. Such assessments inform where to allocate actuation effort, how to prioritize interventions, and how to interpret large-scale models whose state variables may represent heterogeneous quantities. Yet, for many networked systems, it remains challenging to produce node-level importance scores that are both physically meaningful and robust to modeling conventions such as coordinate choices. Moreover, if a large-scale network is actuated through a single node, standard Gramian-based controllability metrics can deteriorate rapidly with the system size, making them numerically unreliable even when the system is controllable [5]. This issue affects node-ranking approaches that evaluate each node in isolation using a single actuation model, as in [4, Section III-G].

Motivated by this challenge, in our prior work [6], we introduced a controllability scoring framework based on a virtual actuation viewpoint and proposed two node-allocation scores: the volumetric controllability score (VCS) and the average-energy controllability score (AECS). The core idea is to conceptually attach one virtual input channel to each

This work was supported by JST PRESTO, Japan, Grant Number JP-MJPR25K4.

TABLE I: Structural equivalence between controllability scoring and approximate OED, and the resulting coordinate invariance properties.

OED	Controllability Score	Coordinate invariance
D-optimal design	VCS	Yes
A-optimal design	AECS	No

state node, distribute a fixed actuation resource across these channels, and interpret the resulting optimal allocation on a probability simplex as a normalized node score. Subsequent work further developed the theory and applications of this framework by establishing a uniqueness result and demonstrating applicability to human brain networks [7], and by extending the formulation to accommodate constraints on actuated nodes [8].

The present paper builds on this framework and addresses two conceptual and practical questions:

- How does controllability scoring relate to classical approximate optimal experimental design (OED) [9]–[12], whose modern formulation dates back to the 1950s [13], [14]?
- How does the network structure encoded in the system matrix govern controllability scores over long time horizons?

The contributions of this paper are summarized as follows:

- i) We clarify the connection between controllability scoring and approximate OED. Under the virtual actuation model, the finite-horizon controllability Gramian admits an additive decomposition across state nodes, yielding an affine matrix model that is structurally identical to the information-matrix model in approximate OED. This establishes a direct correspondence (Table I): VCS corresponds to D-optimality, whereas AECS corresponds to A-optimality. Motivated by this analogy, we further show an invariance gap under state-coordinate changes: VCS is invariant under any nonsingular transformation, while AECS generally depends on the chosen coordinates (and thus can vary with unit changes).
- ii) We highlight a fundamental contrast between approximate OED and controllability scoring. Optimal allocations in approximate OED need not be unique [9], whereas the

controllability-scoring allocation is typically unique [6], [7]. This distinction is crucial because controllability scoring interprets the optimizer itself as centrality-like scores, rather than using the optimal value alone. Moreover, unlike the approximate OED framework, controllability scoring involves an intrinsic time-horizon parameter T through the finite-time controllability Gramian, and the resulting $T \rightarrow \infty$ limit is a distinctive issue specific to controllability scores.

- iii) We provide a structural understanding of how the system matrix (i.e., the network coupling pattern) shapes the AECS allocation over long horizons. In particular, we identify source-like nodes without negative self-loops as a key architectural feature of the system matrix that can systematically drive AECS to downweight the corresponding nodes as the horizon grows. This mechanism is intrinsic to controllability scoring with no direct analogue in approximate OED. We corroborate this behavior in numerical experiments.

The remainder of the paper is organized as follows. We review controllability scoring in Section II. In Section III, we discuss the similarities and differences between controllability scoring and approximate OED. Section IV provides a structural understanding of how the system matrix (i.e., the network coupling pattern) shapes the long-horizon AECS allocation. In particular, it shows that source-like nodes without negative self-loops can be systematically downweighted by AECS as the horizon grows—a mechanism intrinsic to controllability scoring with no direct analogue in approximate OED. Numerical examples illustrating the source-node mechanism described in Section IV are provided in Section V. Finally, Section VI concludes the paper.

Notation: Let \mathbb{N} , \mathbb{R} , and \mathbb{C} denote the sets of natural numbers, real numbers, and complex numbers, respectively. We denote the imaginary unit by i . For a matrix X , X^\top denotes the transpose. For $X \in \mathbb{C}^{m \times n}$, the Hermitian transpose is defined by $X^\dagger := (\overline{X})^\top$, where \overline{X} denotes the elementwise complex conjugate of X . For a square matrix X , $\text{tr}(X)$, $\det(X)$, and $\exp(X)$ denote the trace, determinant, and matrix exponential of X , respectively. We write $X \succeq 0$ (resp., $X \succ 0$) to denote that X is Hermitian positive semidefinite (resp., positive definite). For any matrix $M \in \mathbb{C}^{n \times n}$ and index sets $I, J \subseteq \{1, \dots, n\}$, we denote by $M_{I, J}$ the submatrix with rows in I and columns in J . When $I = \{i\}$ and $J = \{j\}$, we simply write M_{ij} instead of $M_{I, J}$; when $I = \{i\}$ (resp., $J = \{j\}$), $M_{i, J}$ (resp., $M_{I, j}$) denotes the corresponding row (resp., column) submatrix. For a vector x , x_i denotes its i th component. The identity matrix of size n is denoted by I_n . We also write I for an identity matrix of appropriate size when there is no ambiguity. The symbol $\mathbf{1}$ denotes all-ones vector in \mathbb{R}^n , and e_i is the i th standard basis vector. The symbol $\text{diag}(a_1, \dots, a_n)$ denotes the diagonal matrix with diagonal entries a_1, \dots, a_n . For a closed convex set C , $\Pi_C(\cdot)$ denotes

the Euclidean projection onto C . For $k \in \mathbb{N}$, let

$$\Delta_k := \left\{ x \in \mathbb{R}^k \mid \sum_{i=1}^k x_i = 1, x_i \geq 0 \right\}.$$

II. CONTROLLABILITY SCORES

This section recalls the controllability-scoring framework [6]. We start from an autonomous linear-time invariant (LTI) network system

$$\dot{x}(t) = Ax(t), \quad (1)$$

where $x(t) = (x_1(t) \ \dots \ x_n(t))^\top \in \mathbb{R}^n$ and $x_i(t)$ denotes the state of node i . The matrix $A \in \mathbb{R}^{n \times n}$ encodes weighted interactions among nodes. For autonomous dynamics (1), the notion of controllability is not directly applicable because there is no physical input channel. Therefore, following the virtual-actuation viewpoint, we introduce virtual input channels at all state nodes and use them to quantify where to intervene and how strongly.

A. Virtual actuation model and the corresponding controllability Gramian

To define controllability scores, we augment (1) with virtual inputs and consider the following virtually actuated system:

$$\dot{x}(t) = Ax(t) + B(p)u(t), \quad (2)$$

where $B(p) := \text{diag}(\sqrt{p_1}, \dots, \sqrt{p_n})$. This setting establishes a one-to-one correspondence between each state node x_i and a virtual input channel u_i . For any horizon $T > 0$, the finite-time controllability Gramian of (2) is defined as

$$W(p, T) := \int_0^T \exp(At)B(p)B(p)^\top \exp(A^\top t) dt \\ = \sum_{i=1}^n p_i W_i(T), \quad (3)$$

where

$$W_i(T) := \int_0^T \exp(At)e_i e_i^\top \exp(A^\top t) dt.$$

Thus, $W_i(T)$ quantifies the controllability contribution of the single virtual channel acting on node i over $[0, T]$, and $W(p, T)$ is a weighted sum of $W_1(T), \dots, W_n(T)$.

B. Finite-time controllability scoring problem

We define controllability scores as optimal allocations of the virtual actuation budget:

$$\begin{aligned} & \text{minimize} && h_T(p) \\ & \text{subject to} && p \in X_T \cap \Delta_n. \end{aligned} \quad (4)$$

Here, X_T is defined as

$$X_T := \{p \in \mathbb{R}^n \mid W(p, T) \succ O\}.$$

The constraint $p \in X_T$ ensures that virtual system (2) is controllable. Moreover, $p \in \Delta_n$ encodes relative importance

under a fixed budget. The objective function $h_T(p)$ is chosen as either

$$\begin{aligned} f_T(p) &:= -\log \det W(p, T), \\ g_T(p) &:= \text{tr}(W(p, T)^{-1}). \end{aligned} \quad (5)$$

When $h_T = f_T$, any optimizer of Problem (4) is called a volumetric controllability score (VCS); when $h_T = g_T$, any optimizer of Problem (4) is called an average-energy controllability score (AECS). Intuitively, VCS promotes enlarging the controllability ellipsoid, whereas AECS promotes reducing the average control energy. In both cases, the optimizer is interpreted as a node-level centrality score: a larger p_i assigns more virtual actuation authority (i.e., a larger share of the intervention budget) to node i , indicating that intervening at that node is expected to be more effective in influencing the network dynamics over $[0, T]$.

C. Algorithm for solving Problem (4)

Problem (4) can be solved using a projected-gradient method with projections onto the simplex Δ_n . We refer to [6], [7] for algorithmic details and convergence guarantees.

Remark 1: Unlike classical control problems, controllability scoring is motivated by networked systems (e.g., brain or social networks) where designing and applying continuous control inputs is often infeasible. Interventions are instead implemented through high-level actions such as policies, resource allocations, or localized treatments, rather than engineered actuators. Accordingly, the goal of controllability scoring is not controller synthesis but intervention planning: identifying where limited intervention capability should be placed to most effectively influence the network dynamics.

III. RELATION BETWEEN PROBLEM (4) AND OPTIMAL EXPERIMENTAL DESIGN

This section clarifies the relationship between controllability scoring and classical optimal experimental design (OED) [11].

A. Approximate OED

We briefly recall the classical setting of approximate OED in linear regression; see, e.g., [9]. Consider the model

$$y = F\theta + \varepsilon, \quad y \in \mathbb{R}^N, \quad \theta \in \mathbb{R}^d,$$

where the i th row of F is the regression vector $f(x_i)^\top$ associated with an experimental condition x_i and ε is a zero-mean Gaussian noise vector with covariance $\sigma^2 I_N$. Suppose that there are m distinct conditions x_1, \dots, x_m and that condition x_i is used k_i times, so that $N = \sum_{i=1}^m k_i$ and $w_i := k_i/N$ defines the empirical design weights $w \in \Delta_m$.

The least-squares estimator $\hat{\theta} = (F^\top F)^{-1} F^\top y$ is unbiased with covariance $\sigma^2 (F^\top F)^{-1}$. The Fisher information matrix is therefore

$$M(w) := \frac{1}{\sigma^2} F^\top F = \frac{N}{\sigma^2} \sum_{i=1}^m w_i f(x_i) f(x_i)^\top = \sum_{i=1}^m w_i M_i,$$

where $M_i := \frac{N}{\sigma^2} f(x_i) f(x_i)^\top$ are the elementary information matrices.

TABLE II: Structural correspondence between Problem (4) and Problem (6).

Problem (4)	Problem (6)
p	w
$W_i(T)$	M_i
$f_T(p)$	$\alpha(w)$
$g_T(p)$	$\beta(w)$

Based on the information matrix $M(w)$, approximate OED problems can be formulated as

$$\begin{aligned} &\text{minimize} && \gamma(w) \\ &\text{subject to} && w \in \Delta_m. \end{aligned} \quad (6)$$

Here, the objective function $\gamma(w)$ is chosen as either

$$\alpha(w) := -\log \det M(w), \quad \beta(w) := \text{tr}(M(w)^{-1}).$$

When $\gamma = \alpha$, any minimizer w^* is called a D-optimal design; when $\gamma = \beta$, any minimizer w^* is called an A-optimal design.

Problem (6) is directly comparable to Problem (4); see Table II for the correspondence. Unlike Problem (4), where $p \in X_T$ explicitly enforces $W(p, T) \succ O$, Problem (6) is often written only with the simplex constraint $w \in \Delta_m$. Note that this correspondence is structural rather than semantic, as explained in Section III-C1.

B. Invariance of VCS and coordinate dependence of AECS

It is well known in OED [11] that D-optimality is invariant under nonsingular reparameterizations, whereas A-optimality generally depends on the chosen coordinates. As suggested by Table II, we show that the same phenomenon arises for controllability scoring under state-coordinate changes: VCS is invariant, while AECS is not in general.

Consider the state-coordinate change (including rescalings)

$$x = S\tilde{x}, \quad (7)$$

where $S \in \mathbb{C}^{n \times n}$ is any nonsingular (possibly complex-valued) matrix. Then, virtual system (2) is rewritten as

$$\dot{\tilde{x}}(t) = \tilde{A}\tilde{x}(t) + \tilde{B}(p)u(t), \quad (8)$$

where $\tilde{A} := S^{-1}AS$ and $\tilde{B}(p) := S^{-1}B(p)$. The corresponding finite-time controllability Gramian satisfies the standard congruence relation

$$\widetilde{W}(p, T) = S^{-1}W(p, T)S^{-\dagger}. \quad (9)$$

This implies that

$$\widetilde{W}(p, T) \succ O \Leftrightarrow W(p, T) \succ O.$$

Thus, the feasibility of Problem (4) is unaffected by coordinate-change (7).

Accordingly, the counterpart of Problem (4) under (7) is formulated as

$\begin{aligned} & \text{minimize} && \tilde{h}_T(p) \\ & \text{subject to} && p \in X_T \cap \Delta_n. \end{aligned} \tag{10}$

The objective function $\tilde{h}_T(p)$ is chosen as either

$$\begin{aligned} \tilde{f}_T(p) &:= -\log \det \widetilde{W}(p, T), \\ \tilde{g}_T(p) &:= \text{tr}(\widetilde{W}(p, T)^{-1}). \end{aligned} \tag{11}$$

The following proposition shows that VCS is invariant under nonsingular state-coordinate transformations, familiar from D-optimal design. Consequently, the VCS-induced node scoring is robust against coordinate changes.

Proposition 1 (VCS invariance): Let $A \in \mathbb{R}^{n \times n}$ be arbitrary and let $S \in \mathbb{C}^{n \times n}$ be any nonsingular matrix. Let p_{VCS} be an optimal solution to Problem (4) with $h_T = f_T$ for system (2), and let \tilde{p}_{VCS} be an optimal solution to Problem (10) with $\tilde{h}_T = \tilde{f}_T$ for system (8). Then,

$$\tilde{p}_{\text{VCS}} = p_{\text{VCS}}. \tag{12}$$

Moreover, for almost all $T > 0$, the optimal solution to Problem (10) with $\tilde{h}_T = \tilde{f}_T$ is unique.

Proof: It follows from (9) and (11) that

$$\begin{aligned} \tilde{f}_T(p) &= -\log \det(S^{-1}W(p, T)S^{-\dagger}) \\ &= f_T(p) + 2 \log |\det S|. \end{aligned}$$

Since the second term is independent of p , (12) holds. The almost-everywhere uniqueness follows immediately from [7, Theorem 1]. \square

In contrast, the following example shows that AECS can be sensitive to a state-coordinate change. In heterogeneous networks, the sensitivity is not a minor technicality: it can alter node rankings even when the underlying dynamics are unchanged.

Example 1: Let $n = 2$, $A = 0$, and fix any $T > 0$. Then $\exp(At) = I_2$ and, for $p = (p_1, p_2) \in \Delta_2$,

$$W(p, T) = \int_0^T B(p)B(p)^\top dt = T \text{diag}(p_1, p_2).$$

Thus, the constraint $p \in X_T$ yields

$$\text{tr}(W(p, T)^{-1}) = \frac{1}{T} \left(\frac{1}{p_1} + \frac{1}{p_2} \right).$$

The Lagrange multiplier method implies that

$$(p_1, p_2) = (1/2, 1/2) \tag{13}$$

is the optimal solution, i.e., AECS.

Next, consider the diagonal scaling, i.e., a state-coordinate change, $x = S\tilde{x}$ with $S = \text{diag}(s_1, s_2)$ where $s_1 > 0$ and $s_2 > 0$ ($s_1 \neq s_2$). Then, (9) yields

$$\widetilde{W}(p, T) = T \text{ diag}\left(\frac{p_1}{s_1^2}, \frac{p_2}{s_2^2}\right),$$

and thus if $p \in X_T$,

$$\text{tr}(\widetilde{W}(p, T)^{-1}) = \frac{1}{T} \left(\frac{s_1^2}{p_1} + \frac{s_2^2}{p_2} \right),$$

and the Lagrange multiplier method implies that

$$(p_1, p_2) = \left(\frac{s_1}{s_1 + s_2}, \frac{s_2}{s_1 + s_2} \right),$$

which differs from (13) whenever $s_1 \neq s_2$. Thus, the AECS optimizer is not invariant under nonsingular state-coordinate changes in general. \square

Remark 2 (On transpose vs. Hermitian transpose): In the real-valued setting, the finite-time controllability Gramian $W(p, T)$ is defined as (3). However, if we allow complex-valued state-coordinate change (7), then (3) must be interpreted with the transpose replaced by the Hermitian transpose:

$$W(p, T) = \int_0^T \exp(At)B(p)B^\dagger(p)\exp(A^\dagger t) dt,$$

so that $W(p, T)$ is Hermitian and positive semidefinite, consistent with the standard energy inner product $\langle z, w \rangle = z^\dagger w$ on \mathbb{C}^n . This distinction is essential: keeping $^\top$ while allowing complex S can destroy positive definiteness under a coordinate change. For instance, for any $W \succ 0$ and $S = iI$,

$$S^{-1}WS^{-\top} = (-i)W(-i) = -W \prec 0,$$

whereas

$$S^{-1}WS^{-\dagger} = (-i)W(i) = W \succ 0.$$

C. Difference

Although Problem (4) and Problem (6) are identical in optimization form up to the extra feasibility constraint $p \in X_T$ in Problem (4), they differ in several important respects.

These differences are crucial for our controllability-based interpretation.

1) *Different semantics:* In Problem (4), the weights $p \in \Delta_n$ are assigned one-to-one to the state nodes of a fixed dynamical network and are interpreted as normalized controllability-based centrality scores. Controllability scoring is inherently shaped by the system matrix A : the network-induced propagation encoded in $\exp(At)$ couples the design weights across nodes, and structural features of A (such as source-like nodes) can strongly influence the optimizer. This mechanism is also time-scale dependent, because the horizon parameter T directly changes how far and how strongly actuation effects can spread through the network, which in turn can yield qualitatively different allocations under VCS and AECS, as detailed in Sections IV and V.

Problem (6) is conceptually different. The weights $w \in \Delta_m$ represent the relative frequencies with which candidate experimental conditions x_i are used to estimate an unknown parameter vector $\theta \in \mathbb{R}^d$ in a specified regression model, and the information matrix $M(w)$ summarizes the accuracy of parameter estimation. Unlike Problem (4), Problem (6) does not involve network-induced state propagation, a system matrix governing inter-node flow, or a time-horizon parameter.

2) *Uniqueness*: In Problem (6), the parameter dimension d is often moderate, while the number of candidate design points m can be large. Each M_i is a symmetric $d \times d$ matrix and therefore lies in the $d(d+1)/2$ -dimensional vector space of symmetric matrices. It is thus common for $\{M_i\}_{i=1}^m$ to be linearly dependent. Consequently, the set of optimal approximate designs is often not a single point but a nontrivial polytope of optimal weights, as analyzed in [9]. In particular, D- or A-optimal designs are typically not unique.

In controllability scoring, we instead aggregate the finite-time controllability contributions $W_i(T)$ associated with the virtual inputs at the state nodes. Here, the number of design variables equals the state dimension n , and the matrices $\{W_i(T)\}_{i=1}^n$ are generically linearly independent. Consequently, the optimal allocations defining VCS and AECS are typically unique [7, Theorem 1], which is crucial for interpreting them as centrality-like scores for the state nodes.

3) *Intrinsic time horizon T and the limit $T \rightarrow \infty$* : Unlike Problem (6), controllability scoring problem (4) involves an intrinsic time-horizon parameter $T > 0$ through finite-time controllability Gramian $W(p, T)$ defined by (3). The limit $T \rightarrow \infty$ is a new issue in controllability scoring, as it removes dependence on a user-chosen terminal time and thereby improves reproducibility. However, this limit cannot be addressed by the standard Gramian-based approach when A is non-Hurwitz: the controllability Gramian $W(p, T)$ diverges as $T \rightarrow \infty$, and even for large finite T it can become severely ill-conditioned, making the objective functions numerically unstable and rendering many Gramian-based centralities ill-defined on an infinite horizon.

Recent work [15] resolves this obstacle by introducing a scaled controllability Gramian that compensates for the contributions of unstable modes. This can be regarded as state-coordinate change (7) with

$$S = QD(T),$$

where Q is an invertible matrix that brings A into its Jordan normal form and $D(T)$ is a block-diagonal, time-dependent scaling. This scaling yields optimization problems equivalent to the original finite-horizon ones but numerically stable for large T , and it enables taking $T \rightarrow \infty$ in a mathematically meaningful way, resulting in well-posed infinite-horizon controllability scores. Moreover, under suitable assumptions, the finite-horizon scores are shown to converge to these unique infinite-horizon limits, thereby providing a principled choice of the terminal time, namely $T = \infty$.

IV. WHY AECS DOWNWEIGHTS SOURCE-LIKE NODES ON LONG HORIZONS

This section provides a structural explanation for why AECS can yield node rankings that differ qualitatively from those induced by VCS on long horizons, as reported in [7, Section III-C-3]. The key mechanism is the presence of source-like state nodes, i.e., coordinates that are weakly affected by the rest of the network. For such nodes, a diagonal entry of the finite-time controllability Gramian $W(p, T)$ defined by

(3) admits an explicit form, leading to sharp lower bounds for AECS and revealing a characteristic contrast to the VCS behavior on long horizons. Importantly, this mechanism is specific to controllability scoring (Problem 4) and has no direct counterpart in classical OED (Problem 6), as mentioned in Section III-C-1.

A. Explicit formula for the diagonal Gramian entry under a left-eigenvector condition

We start from a structural condition that captures “source-like” behavior at the level of the system matrix A .

Assumption 1 (Left-eigenvector condition): Fix an index $i \in \{1, \dots, n\}$. Assume that there exists $\ell_i \in \mathbb{R}$ such that

$$e_i^\top A = \ell_i e_i^\top, \quad (14)$$

i.e., e_i is a left eigenvector of A .

Assumption 1 means that the i th row of A has no off-diagonal entries: $A_{ij} = 0$ for all $j \neq i$. In particular, the scalar ℓ_i in (14) is simply the diagonal entry, $\ell_i = A_{ii}$. Thus, x_i is not driven by other state nodes. In this sense, x_i behaves as a source-like node, and the sign of ℓ_i specifies whether it has a nonnegative self-loop weight.

Lemma 1: Suppose that Assumption 1 holds. Then, the (i, i) entry of $W(p, T)$ is given by

$$(W(p, T))_{ii} = p_i \omega_i(T), \quad (15)$$

where

$$\omega_i(T) = \begin{cases} T & \text{if } \ell_i = 0, \\ \frac{e^{2\ell_i T} - 1}{2\ell_i} & \text{if } \ell_i \neq 0. \end{cases} \quad (16)$$

Proof : By definition (3),

$$\begin{aligned} (W(p, T))_{ii} &= e_i^\top W(p, T) e_i \\ &= \int_0^T e_i^\top \exp(At) \text{diag}(p) \exp(A^\top t) e_i dt \\ &= p_i \int_0^T e^{2\ell_i t} dt. \end{aligned}$$

The third equality follows from Assumption 1, which implies $e_i^\top \exp(At) = e^{\ell_i t} e_i^\top$. Thus, (15) holds. \square

B. AECS lower bound

We provide a quantitative lower bound for the AECS objective function $g_T(p)$ in Problem (4).

Theorem 1: Suppose that $p \in X_T$ and Assumption 1 hold. Then,

$$g_T(p) \geq \frac{1}{p_i \omega_i(T)}, \quad (17)$$

where ω_i is defined by (16).

Proof : By definition (5) of g_T ,

$$g_T(p) \geq (W(p, T)^{-1})_{ii} \geq \frac{1}{(W(p, T))_{ii}}.$$

The first inequality follows from the definition of the trace. The second inequality follows from Lemma 3 in Appendix A. Thus, Lemma 1 yields (17). \square

A particularly revealing case is $\ell_i = 0$, for which $\omega_i(T) = T$ in (15). Then, (17) becomes

$$g_T(p) \geq \frac{1}{p_i T}. \quad (18)$$

Thus, for any fixed $p_i > 0$, this lower bound decays as T^{-1} as $T \rightarrow \infty$. Equivalently, the lower bound becomes less restrictive on long horizons, which helps explain why the AECS optimizer may allocate a very small weight to a source-like node when T is large.

In contrast, if $\ell_i < 0$, (17) yields the non-decaying bound

$$g_T(p) \geq \frac{-2\ell_i}{p_i(1-e^{2\ell_i T})} \rightarrow \frac{-2\ell_i}{p_i} \quad (T \rightarrow \infty). \quad (19)$$

Hence, unlike the marginal case $\ell_i = 0$, strictly stable self-dynamics remove the horizon-induced relaxation of the lower bound and thus discourage the AECS optimizer from taking p_i extremely small. In fact, (19) shows that making p_i very small forces $g_T(p)$ to be large, so such allocations are penalized by the AECS objective.

Remark 3: If $\ell_i > 0$, (17) yields

$$g_T(p) \geq \frac{2\ell_i}{p_i(e^{2\ell_i T} - 1)}.$$

As $T \rightarrow \infty$, the right-hand side decays exponentially. Thus, the lower bound becomes even less restrictive than in the marginal case $\ell_i = 0$. Accordingly, this bound alone does not prevent the AECS optimizer from taking p_i very small on long horizons.

C. VCS lower bound

Unlike the AECS objective function g_T , the VCS objective f_T does not reduce to a bound in terms of $p_i \omega_i(T)$ alone:

Theorem 2: Suppose that $p \in X_T$ and Assumption 1 hold. Then,

$$f_T(p) \geq -\log(p_i \omega_i(T)) - \log \det(W(p, T))_{\bar{i}, \bar{i}}, \quad (20)$$

where $\bar{i} := \{1, \dots, n\} \setminus \{i\}$ and ω_i is defined in (16).

Proof: Since $p \in X_T$, $W(p, T) \succ 0$. Thus, Lemma 2 in Appendix A implies that

$$\det W(p, T) \leq (W(p, T))_{ii} \det((W(p, T))_{\bar{i}, \bar{i}}).$$

Thus, Lemma 1 yields (20). \square

The bound (20) makes explicit that the lower bound of f_T depends on p_i not only through $-\log(p_i \omega_i(T))$ but also through the term $-\log \det(W(p, T))_{\bar{i}, \bar{i}}$, which depends on the overall allocation p . Consequently, Assumption 1 alone does not justify the conclusion that choosing p_i small is beneficial for VCS on long horizons.

V. EXAMPLES

This section illustrates the qualitative discrepancy between VCS and AECS by two examples. We first present a minimal two-node model, for which the finite-time Gramian admits a closed-form expression. We then revisit the $n = 10$ directed network used in our earlier numerical study [7] to demonstrate that the same phenomenon appears in a larger network.

A. A closed-form two-node diagonal example

We consider the 2×2 diagonal dynamics (2) with

$$A = \begin{pmatrix} 0 & 0 \\ 0 & -1 \end{pmatrix}. \quad (21)$$

Both nodes are source-like in the sense of Assumption 1, since each row of A has no off-diagonal entries and hence

$$e_1^\top A = 0 \cdot e_1^\top, \quad e_2^\top A = (-1) \cdot e_2^\top.$$

In particular, node 1 is marginal ($\ell_1 = 0$), whereas node 2 is strictly stable ($\ell_2 = -1$). For this system, the finite-time controllability Gramian $W(p, T)$ defined in (3) is given by

$$W(p, T) = \begin{bmatrix} p_1 T & 0 \\ 0 & p_2 \zeta(T) \end{bmatrix}, \\ \zeta(T) := \int_0^T e^{-2t} dt = \frac{1 - e^{-2T}}{2}.$$

Note that $p = (p_1, p_2) \in X_T \cap \Delta_2$ implies that $0 < p_1, p_2 < 1$.

1) *VCS:* Since A in (21) is symmetric, [7, Theorem 2] implies that the unique VCS optimizer is

$$(p_1^{\text{VCS}}(T), p_2^{\text{VCS}}(T)) = (1/2, 1/2)$$

for all $T > 0$.

2) *AECS:* By (5), for $p = (p_1, p_2) \in X_T \cap \Delta_2$,

$$g_T(p) = \frac{1}{Tp_1} + \frac{1}{p_2 \zeta(T)}.$$

Thus, the Lagrange multiplier method yields the unique AECS optimizer

$$p_1^{\text{AECS}}(T) = \frac{1}{1 + \sqrt{\frac{2T}{1 - e^{-2T}}}}, \\ p_2^{\text{AECS}}(T) = 1 - p_1^{\text{AECS}}(T).$$

In particular, $p_1^{\text{AECS}}(T) \rightarrow 0$ as $T \rightarrow \infty$. This illustrates, in the simplest closed form, how a source-like node with a nonnegative self-loop can be assigned vanishing weight in the AECS objective function g_T on long horizons, in contrast to the VCS objective function f_T .

B. 10-node directed network examples

We next consider the directed network in Fig. 1, originally studied in [7, Section III-C-3], to illustrate how the long-horizon behavior of the scores depends on the presence of self-loops at source-like nodes.

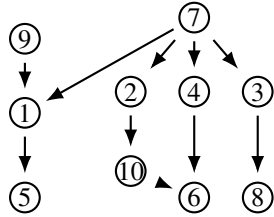


Fig. 1: Network employed in the numerical experiments.

1) *Source-like nodes without self-loops*: The network in Fig. 1 consists of $n = 10$ nodes and all edges have a uniform weight $c = 0.2$. Let L denote the (directed) graph Laplacian associated with this network and set $A = -L$.

This network contains two source-like nodes (nodes 7 and 9) in the sense that they have no incoming edges, and hence their corresponding rows of $A = -L$ have no off-diagonal entries. In particular, both nodes satisfy Assumption 1 with $\ell_i = A_{ii} = 0$. The marginal case $\ell_i = 0$ yields the lower bound (18).

Table III shows that this mechanism manifests sharply for node 9: its AECS allocation drops from 9.1×10^{-2} at $T = 1$ to 7.0×10^{-3} at $T = 1000$ and further to 2.3×10^{-3} at $T = 10000$. By contrast, the AECS allocation of node 7 remains bounded away from zero even for $T = 10000$. This disparity is consistent with the network topology. Although both nodes are source-like in the sense of having no incoming edges, node 7 has multiple outgoing edges (it directly influences nodes 1–4), so allocating actuation budget to node 7 improves the reachability of several downstream states and continues to reduce the average control energy captured by $g_T(p)$. Node 9, in contrast, has a more limited downstream reach in this topology (it primarily feeds into node 1 and then node 5). Since the virtual-actuation model allows direct allocation to other nodes, comparable downstream improvements can often be achieved by allocating budget elsewhere, which is consistent with the strong downweighting of node 9 under AECS for large T .

VCS exhibits the opposite behavior on long horizons. While the allocations are nearly uniform for very short horizons ($T = 0.01$), VCS increasingly concentrates weight on upstream (source-like) nodes as T increases, assigning substantial mass to nodes 7 and 9 (approximately 0.249 and 0.166, respectively, at $T = 10000$). This contrast can be traced back to the distinct analytic structures of the two objectives. In fact, the VCS objective function f_T does not admit an analogous reduction to a bound depending only on $p_i \omega_i(T)$ as in (18): Under Assumption 1, (20) shows that the influence of p_i on f_T remains coupled to the overall allocation through the principal submatrix determinant term. As a result, even when a node is source-like, VCS need not favor driving its allocation toward zero on long horizons, which is consistent with the non-negligible VCS weights observed for nodes 7 and 9 in Table III.

2) *Source-like nodes with negative self-loops*: We next consider a self-loop variant of the network in Fig. 1. The

underlying directed topology and all off-diagonal edge weights remain unchanged; the only modification is the addition of a negative self-loop at node 9: We replaced the $(9, 9)$ entry by $A_{99} = -1$ while keeping A_{ij} unchanged for all $(i, j) \neq (9, 9)$.

Table IV shows that once a negative self-loop is added at node 9, the AECS assigns the largest weight to node 9 on long horizons; $p_9^{\text{AECS}} \approx 0.195$ for $T = 10000$, in sharp contrast to the no-self-loop case where the same node can be strongly downweighted. This behavior is consistent with our theoretical analysis: when a source-like node has a negative self-loop (i.e., $\ell_i < 0$), the lower bound of AECS objective function g_T no longer relaxes with the horizon, but instead remains bounded away from zero as $T \rightarrow \infty$; see (19). Consequently, driving the corresponding allocation p_i to be very small would incur a large g_T , and the optimizer is discouraged from assigning a near-zero weight.

VI. CONCLUSION

This paper clarified the structure and interpretation of controllability scoring for networked dynamical systems. Under a node-wise virtual actuation model, the finite-time controllability Gramian decomposes additively across state nodes, yielding an affine matrix model that matches the information-matrix model in approximate OED; consequently, VCS and AECS correspond to the D- and A-optimal design criteria, and the classical D/A coordinate-invariance gap carries over under state-coordinate changes (VCS is invariant under any nonsingular transformation, whereas AECS is not in general). We also emphasized a key distinction from approximate OED: while OED optima need not be unique, controllability scoring typically admits a unique optimal allocation, which is essential because the optimizer itself is interpreted as a node-level importance score. Finally, we identified a long-horizon phenomenon with no OED analogue: AECS can strongly downweight source-like nodes when their self-dynamics are weak, whereas VCS need not due to its determinant-based coupling; when source-like nodes have negative self-loops, this tendency is mitigated and AECS can behave closer to VCS. Numerical examples corroborated these trends and showed that AECS and VCS can yield qualitatively different node scores on long horizons.

APPENDIX

A. Technical lemmas for VCS and AECS lower bounds

This appendix collects two elementary matrix inequalities that we use to derive lower bounds for f_T and g_T . Lemma 2 provides an upper bound on $\det W$. Lemma 3 gives a convenient lower bound on the diagonal entries of W^{-1} . These inequalities are standard; see, e.g., [16]. For the sake of a self-contained presentation, we include short proofs here.

Lemma 2: Let $W \in \mathbb{R}^{n \times n}$ be symmetric and positive definite. Then, for each $i \in \{1, \dots, n\}$,

$$\det W \leq W_{ii} \det(W_{\bar{i}, \bar{i}}) \quad (22)$$

holds, where $\bar{i} := \{1, \dots, n\} \setminus \{i\}$.

TABLE III: Evaluation of VCS and AECS for various T reported in [7, Table III].

VCS					AECS				
Node	$T = 0.01$	$T = 1$	$T = 1000$	$T = 10000$	Node	$T = 0.01$	$T = 1$	$T = 1000$	$T = 10000$
1	0.1000	0.0997	0.0733	0.0733	1	0.1000	0.1093	0.1713	0.1728
2	0.1000	0.1000	0.1011	0.1011	2	0.1000	0.1000	0.1133	0.1136
3	0.1000	0.1000	0.1088	0.1087	3	0.1000	0.1000	0.1205	0.1209
4	0.1000	0.1000	0.0864	0.0864	4	0.1000	0.1000	0.1058	0.1061
5	0.1000	0.0997	0.0456	0.0450	5	0.1000	0.0998	0.0907	0.0923
6	0.1000	0.0994	0.0607	0.0607	6	0.1000	0.1091	0.1335	0.1338
7	0.1000	0.1013	0.2493	0.2495	7	0.1000	0.0913	0.0926	0.0928
8	0.1000	0.0997	0.0423	0.0422	8	0.1000	0.0998	0.0695	0.0694
9	0.1000	0.1003	0.1661	0.1667	9	0.1000	0.0908	0.0070	0.0023
10	0.1000	0.1000	0.0664	0.0663	10	0.1000	0.1000	0.0957	0.0959

 TABLE IV: Evaluation of VCS and AECS for various T on the 10-node directed network in Fig. 1, where the only modification from the no-self-loop case is a negative self-loop of weight -1 added at node 9 (i.e., $A_{99} = -1$).

VCS					AECS				
Node	$T = 0.01$	$T = 1$	$T = 1000$	$T = 10000$	Node	$T = 0.01$	$T = 1$	$T = 1000$	$T = 10000$
1	0.1000	0.0997	0.0974	0.0974	1	0.1000	0.1044	0.1269	0.1269
2	0.1000	0.1000	0.1020	0.1020	2	0.1000	0.0955	0.0938	0.0938
3	0.1000	0.1000	0.1096	0.1096	3	0.1000	0.0955	0.1001	0.1001
4	0.1000	0.1000	0.0874	0.0874	4	0.1000	0.0955	0.0872	0.0872
5	0.1000	0.0997	0.0837	0.0837	5	0.1000	0.0953	0.0739	0.0739
6	0.1000	0.0993	0.0606	0.0605	6	0.1000	0.1044	0.1108	0.1108
7	0.1000	0.1013	0.2490	0.2492	7	0.0999	0.0870	0.0763	0.0763
8	0.1000	0.0997	0.0419	0.0418	8	0.1000	0.0953	0.0570	0.0569
9	0.1000	0.1003	0.1022	0.1022	9	0.1003	0.1316	0.1953	0.1953
10	0.1000	0.1000	0.0661	0.0661	10	0.1000	0.0955	0.0787	0.0787

Proof : Let Π be a permutation matrix that moves the i th coordinate to the first position, and set $\widetilde{W} := \Pi W \Pi^\top$. Then $\widetilde{W} \succ 0$, $\det \widetilde{W} = \det W$, and \widetilde{W} admits the block partition

$$\widetilde{W} = \begin{bmatrix} W_{ii} & W_{i,\bar{i}} \\ W_{\bar{i},i} & W_{\bar{i},\bar{i}} \end{bmatrix}.$$

By the Schur complement formula,

$$\det W = \det \widetilde{W} = W_{ii} \cdot \det(W_{\bar{i},\bar{i}} - W_{\bar{i},i}W_{ii}^{-1}W_{i,\bar{i}}),$$

where the Schur complement $W_{\bar{i},\bar{i}} - W_{\bar{i},i}W_{ii}^{-1}W_{i,\bar{i}} \succ 0$. Moreover, since $W_{\bar{i},i}W_{ii}^{-1}W_{i,\bar{i}} \succeq 0$, we have

$$W_{\bar{i},\bar{i}} - W_{\bar{i},i}W_{ii}^{-1}W_{i,\bar{i}} \preceq W_{\bar{i},\bar{i}},$$

and hence (22) holds. \square

Lemma 3: Let $W \in \mathbb{R}^{n \times n}$ be symmetric and positive definite. Then, for each $i \in \{1, \dots, n\}$,

$$(W^{-1})_{ii} \geq \frac{1}{W_{ii}}. \quad (23)$$

Proof : By the adjugate formula, $(W^{-1})_{ii} = \frac{(\text{adj}(W))_{ii}}{\det W}$. The (i, i) -entry of the adjugate matrix $\text{adj}(W)$ equals the (i, i) -cofactor, and hence $(\text{adj}(W))_{ii} = (-1)^{i+i} \det(W_{\bar{i},\bar{i}}) = \det(W_{\bar{i},\bar{i}})$, where $\bar{i} := \{1, \dots, n\} \setminus \{i\}$. Therefore, $(W^{-1})_{ii} = \frac{\det(W_{\bar{i},\bar{i}})}{\det W}$, and Lemma 2 yields (23). \square

REFERENCES

[1] N. Bof, G. Baggio, and S. Zampieri, “On the role of network centrality in the controllability of complex networks,” *IEEE Transactions on Control of Network Systems*, vol. 4, no. 3, pp. 643–653, 2017.

[2] Y.-Y. Liu, J.-J. Slotine, and A.-L. Barabási, “Controllability of complex networks,” *Nature*, vol. 473, no. 7346, pp. 167–173, 2011.

[3] F. Pasqualetti, S. Zampieri, and F. Bullo, “Controllability metrics, limitations and algorithms for complex networks,” *IEEE Transactions on Control of Network Systems*, vol. 1, no. 1, pp. 40–52, 2014.

[4] T. H. Summers, F. L. Cortesi, and J. Lygeros, “On submodularity and controllability in complex dynamical networks,” *IEEE Transactions on Control of Network Systems*, vol. 3, no. 1, pp. 91–101, 2016.

[5] G. Baggio and S. Zampieri, “Controllability of large-scale networks: The control energy exponents,” *IEEE Transactions on Control of Network Systems*, vol. 11, no. 2, pp. 808–820, 2024.

[6] K. Sato and S. Terasaki, “Controllability scores for selecting control nodes of large-scale network systems,” *IEEE Transactions on Automatic Control*, vol. 69, no. 7, pp. 4673–4680, 2024.

[7] K. Sato and R. Kawamura, “Uniqueness Analysis of Controllability Scores and Their Application to Brain Networks,” *IEEE Transactions on Control of Network Systems*, vol. 12, no. 4, pp. 2568–2580, 2025.

[8] K. Sato, “Target controllability score,” 2025. [Online]. Available: <https://arxiv.org/abs/2510.13354>

[9] R. Harman, L. Filová, and S. Rosa, “The polytope of optimal approximate designs: extending the selection of informative experiments,” *Statistics and Computing*, vol. 34, no. 6, p. 211, 2024.

[10] X. Huan, J. Jagalur, and Y. Marzouk, “Optimal experimental design: Formulations and computations,” *Acta Numerica*, vol. 33, pp. 715–840, 2024.

[11] F. Pukelsheim, *Optimal design of experiments*. SIAM, 2006.

[12] B. Jones, K. Allen-Moyer, and P. Goos, “A-optimal versus d-optimal design of screening experiments,” *Journal of Quality Technology*, vol. 53, no. 4, pp. 369–382, 2021.

[13] G. Elfving, “Optimum allocation in linear regression theory,” *The Annals of Mathematical Statistics*, pp. 255–262, 1952.

[14] J. Kiefer, “Optimum experimental designs,” *Journal of the Royal Statistical Society: Series B (Methodological)*, vol. 21, no. 2, pp. 272–304, 1959.

[15] K. Umezawa and K. Sato, “Infinite-horizon controllability scores for linear time-invariant systems,” *arXiv preprint arXiv:2601.10260*, 2026.

[16] F. Zhang, *The Schur complement and its applications*. Springer Science & Business Media, 2006, vol. 4.